Clim Dyn
DOI 10.1007/s00382-011-0996-2

A parametric sensitivity study of entropy production and kinetic energy dissipation using the FAMOUS AOGCM

Salvatore Pascale · Jonathan M. Gregory ·
Maarten H. P. Ambaum · Rémi Tailleux

Received: 12 October 2010 / Accepted: 12 January 2011

Abstract The possibility of applying either the maximum entropy production conjecture of Paltridge (Q J R Meteorol Soc 101:475–484, 1975) or the conjecture of Lorenz (Generation of available potential energy and the intensity of the general circulation. Pergamon, Tarrytown, 1960) of maximum generation of available potential energy (APE) in FAMOUS, a complex but low-resolution AOGCM, is explored by varying some model parameters to which the simulated climate is highly sensitive, particularly the convective entrainment rate, λ, and cloud droplet-to-rain conversion rate c_T. The climate response is analysed in terms of its entropy production and the strength of the Lorenz energy cycle. If either conjecture is true, the parameter values which yield the most realistic climate will also maximise the relevant quantity. No maximum is found in the total material entropy production, which is dominated by the hydrological cycle and tends to increase monotonically with global-mean temperature, which is not constant because the parameter variations affect the net input of solar radiation at the top of the atmosphere (TOA). In contrast, there is a non-monotonic, peaked behaviour in the generation of APE and entropy production associated with kinetic energy dissipation, with the standard FAMOUS values for λ and c_T occurring nearly at the maximising ones. The maximum states are shown to be states of vigorous baroclinic activity. The peak in the generation of APE appears to be related to a trade-off between the mean vertical stability and horizontal stratification. Experiments are repeated for a simplified setup in which the net solar input at TOA is fixed. Again a peak in the generation of APE is found in association with the maximum baroclinic activity, but no trade-off of the kind shown by simple climate models is found between meridional heat transport and the meridional temperature gradient. We conclude that the maximum entropy production conjecture does not hold within the climate system when the effects of the hydrological cycle and radiative feedbacks are taken into account, but our experiments provide some evidence in support of the conjecture of maximum APE production (or equivalently maximum dissipation of kinetic energy).

Keywords Maximum entropy production · GCM tuning · Lorenz energy cycle strength · Entropy sensitivity

1 Introduction

Lorenz (1960) proposed that the atmospheric general circulation is organized to maximise kinetic energy dissipation (MKED), or, equivalently, the generation of APE. Similarly Paltridge (1975, 1978) suggested that Earth's climate structure might be explained from a hypothesis of maximum entropy production (MEP). Closely related principles have been popular also in biology and engineering. For example the "maximum power principle", advocated by Odum (1988) for biological systems, is consistent with the maximum dissipation conjecture; the "constructal law" of Bejan and Lorente (2004) is very closely related to MEP as discussed by Kleidon (2009). A broad discussion on the maximizing power generation and transfer for Earth system processes can be found in Kleidon (2010).

S. Pascale (✉) · J. M. Gregory · M. H. P. Ambaum · R. Tailleux
Department of Meteorology, University of Reading, Earley Gate, Reading RG6 6BB, UK
e-mail: s.pascale@reading.ac.uk

J. M. Gregory
Met Office Hadley Centre, Exeter EX1 3PB, UK

Published online: 09 February 2011

Although the general validity of these conjectures is still unclear (for a general review see Martyushev and Seleznev 2006; Kleidon 2009) and a rigorous proof still missing (Dewar 2005; Grinstein and Linsker 2007), MEP has stimulated a re-examination of entropy production in the climate system (Peixoto et al. 1991; Ozawa et al. 2003) and, more generally, of new diagnostic tools based on the second law of thermodynamics (Fraedrich and Lunkeit 2008; Lucarini 2009; Lucarini et al. 2010a; Ambaum 2010; Tailleux 2010). Qualitative evidence has been found in favour of MEP and MKED by several authors (Paltridge 1975, 1978; Rodgers 1976; Schulman 1977; Grassl 1981; Noda and Tokioka 1983; Ozawa and Ohmura 1997; Lorenz et al. 2001; Pujol and Fort 2002; Murakami and Kitoh 2005; Wang et al. 2008). These works have used fairly diverse energy-balance models with no dynamics and greatly simplified physics. This lack of dynamical and physical constraints in such models allows for a wide spanning of climatic states regardless of physical feasibility, of which MEP selects the one with maximum entropy production.

The idea has been proposed of using material entropy production and kinetic energy dissipation (or, equivalently, generation of available potential energy) as objective functions for parameter tuning (Kleidon et al. 2003, 2006; Kleidon 2005; Kunz et al. 2008). Testing MEP by using general circulation models (GCMs) relies on the possibility of producing an ensemble of diversified steady states under the same boundary conditions. In a GCM context these can only be achieved by varying $_{\mathrm{internal}}$ parameters corresponding to processes unresolved at the grid scale (see Sect. 2.3), as pointed out in Kunz et al. (2008) (we distinguish $_{\mathrm{internal}}$ from $_{\mathrm{external}}$ parameters, which are not related to the internal dynamics of the climate system, like the solar constant or the rotation speed of Earth). Since a GCM is highly constrained by its physical formulation, it is not obvious that MEP will apply; this is questioned for instance by Goody (2007).

In principle the case of the two-box model and the case of a GCM could be the same. To understand it better, let us recall how entropy production is maximised in the two box-model used in Lorenz et al. (2001) or shown in Kleidon (2009). The meridional heat transport F_{m} is dynamically unresolved and represented as $F = 2K(T_e - T_p)$, with $T_p; T_e$ temperatures of the "polar" (high latitude) and "equatorial" (low latitude) boxes, and K a diffusivity constant. In the model design K is the only internal parameter; the net insolation $I_{e,p}$ of the equatorial and polar boxes are fixed. Variations of K lead to the set of steady states needed for MEP to operate: $K = 0 \Longrightarrow F = 0; K = \infty \Longrightarrow F = (I_e - I_p)/2$. The former has maximum temperature contrast since there is no meridional heat transport and therefore zero entropy production. The latter eliminates the temperature contrast and thus has the maximum heat transport allowed by the second law of thermodynamics but zero entropy production again. There is a "trade-off" between heat transport and temperature contrast whereby entropy production is maximised in some intermediate state.

In a GCM many more equations are implemented but still unresolved processes are represented in a way analogous to meridional heat transport in the two-box model: the convective entrainment rate, for example, is a number which sets the strengths of turbulent mixing between environmental dry air and the moist convective plume. Like the meridional heat flux in the box-model such turbulent fluxes are not dynamically resolved (they could be in principle if the spatial resolution of the large scale flow was high enough) but only parametrised.

Previous studies of parametric variation to examine the entropy sensitivity in a GCM context have been done by Kleidon et al. (2003), Kleidon (2005), Kleidon et al. (2006) and Kunz et al. (2008). Kleidon et al. (2003) vary the timescale of surface friction (Rayleigh friction parametrisation) in a dry atmospheric general circulation model in which the radiative transfer is parametrised as a Newtonian damping of local temperature relaxation to a prescribed radiative-convective equilibrium profile. Kleidon found a state of maximum entropy production corresponding to the largest conversion of APE into kinetic energy and exhibiting the largest eddy activity in the midlatitudes. Furthermore he showed that such a state results in the most effective transport of heat towards the poles and the least equator-pole temperature difference. Kleidon (2005) first suggested that maximising entropy production could be an efficient tool to tune low-resolution climate models. He performed sensitivity simulations with a dynamic-core (PUMA-1, Fraedrich et al. 2005b) by using different intensity of hyperdiffusion at different model resolutions and showed that there is a maximum in entropy production corresponding to the greatest baroclinic activity. Kleidon et al. (2006) studied the connection between entropy production and the strength of boundary layer exchange by varying the Von Kármán parameter in an atmospheric general circulation model of intermediate complexity (Planet Simulator, Fraedrich et al. 2005a). An idealised model setup was used, in which the amount of absorbed solar radiation and the surface albedo were fixed, and the water cycle completely excluded. They showed that the maximum of entropy production associated with boundary layer dissipation is consistent with the observed value of the Von Kármán parameter of 0.4. Kunz et al. (2008) used a simplified atmospheric general circulation model (SGCM PUMA, Fraedrich et al. 2005b) employing linear parametrizations for diabatic heating, surface friction and horizontal diffusion. They found maxima in entropy

production and kinetic energy dissipation for "optimal" parameter values close to the standard con guration of the model. The authors therefore suggested the use of entropy production and kinetic energy dissipation as objective functions for parameter optimisation. Were this hypothesis true, it would be of great utility, since the presence of empirical parameters in GCMs is a main cause of uncertainty in climate projections (Murphy et al. 2004).

The aforementioned works are the rst attempts to use MEP conjecture as a guide to improve general circulation models. However models used for such a purpose have some big simpli cations. Firstly, the atmospheric models are "dry" i.e. with no water cycle, so the entropy production associated with the hydrological cycle is not accounted for. This is a major limitation since the entropy production associated with the hydrological cycle is the dominant term (Pauluis and Held 2002a, b; Fraedrich and Lunkeit 2008; Pascale et al. 2009; see also Sect. 2.2). Without the hydrological cycle in the model the material entropy production corresponds almost entirely to the one associated with heating due to kinetic energy dissipation. This is why in Kunz et al. (2008) the entropy production and kinetic energy dissipation are practically the same when rescaled. Secondly, only GCMs of low complexity are considered with no physical parametrizations and therefore the climate entropy budget is drastically simpli-ed. Thirdly, all the models have prescribed absorbed solar radiation as a boundary condition, and no cloud and water vapour feedback. This simpli cation helps our understanding but it is a limitation of the original spirit of the works of Paltridge (1975, 1978) and Noda and Tokioka (1983), in which MEP is used to determine cloudiness as well. Recent studies (Paltridge et al. 2007; Wang et al. 2008) con rm the inherent power of MEP in determining the cloud feedback and cloud fraction in climate, therefore permitting the model itself to regulate not only the longwave emission to space but also the amount of shortwave radiation re ected back to space by clouds. According to this point of view, we take the *xed (incoming) insolation* to be the proper boundary condition.

This study extends ideas raised in Kunz et al. (2008) to a complex coupled atmosphere–ocean general circulation model (AOGCM), by performing a range of sensitivity simulations in which we modify some key parameters of the model. In doing this we want to address the following issues: (i) to test the applicability and validity of MEP and MKED in a complex AOGCM; (ii) to highlight differences between material entropy production and kinetic energy dissipation when the whole hydrological cycle is included; (iii) to understand which parameters and which processes are signi cant for MEP; (iv) to understand to what extent MEP may provide an inherent principle for parameter optimisation of GCMs (Kunz et al. 2008).

2 Model and method

2.1 The model: FAMOUS

The AOGCM used in this paper is FAMOUS (FAst Met Of ce/UK Universities Simulator, Jones et al. 2005), of which we are using version FAMOUS-xdbua (Smith et al. 2008). FAMOUS is the low resolution version of HadCM3 (Gordon et al. 2000; Pope et al. 2000), which has been widely used to simulate present day and future climate and compares well with other current AOGCMs of the Coupled Model Intercomparison Project (Reichler and Kim 2008). Let us stress again that the two models are identical, apart from spatial resolution, timesteps, a few resolution-dependent constants and the omission of the scheme for spatial variation of the isopycnal layer thickness diffusivity in the ocean.

HadCM3 and FAMOUS are con gurations of the Met Of ce (UK) uni ed forecast and climate model. Apart from some minor differences the physics and the dynamics are the same. By virtue of the reduced horizontal and vertical resolution and increased timestep FAMOUS runs about ten times faster than HadCM3. This characteristic is particularly useful for long runs or large ensembles of integrations, such as in the present work, for which HadCM3 is too expensive in terms of time and resources. However, the reduced resolution means inevitably that the climate in FAMOUS is somewhat less realistic, though still satisfactory for our investigative purposes.

2.1.1 The atmosphere

The atmosphere model of FAMOUS has a horizontal grid spacing of $5 \times 7{:}5^{\circ}$ and 11 vertical levels. A timestep of 1 h is used.

The dynamic core is a split-explicit *nite difference scheme (Cullen and Davies 1991). The prognostic variables are the zonal and meridional wind component, the surface pressure, the speci c humidity and the potential air temperature. Hyperdiffusion is applied after the advection to the model prognostics for numerical stability. The advection should be a fully adiabatic process but the numerical scheme introduces spurious numerically generated entropy sources/sinks (Egger 1999; Johnson 1997).

The physical parametrisation schemes include: (a) the radiation scheme (Edwards and Slingo 1996), (b) the convection scheme (Gregory and Rowntree 1990), (c) the large-scale cloud scheme (Smith 1990), (d) the large-scale precipitation scheme (Gregory 1995), (e) the boundary layer scheme (Smith 1990). The atmosphere model includes the surface model, over both land and ocean, which simulates surface *uxes of latent and sensible heat and momentum i.e. windstress.

2.1.2 The ocean

The ocean component of FAMOUS is a 20 level version of the Cox (1984) model on a $2.5^\circ \times 3.75^\circ$ latitude-longitude grid with a 12 hour time step. The Boussinesq approximation is adopted, in which density differences are neglected except in the buoyancy term of the equation of horizontal motion. The hydrostatic assumption is made in which local acceleration and other terms of equal order are eliminated from the equation of vertical motion. The prognostic variables are sea-water potential temperature, salinity and horizontal velocity. Within the ocean various parametrisation schemes are employed to represent small-scale turbulent mixing including convection.

The atmospheric and ocean model are coupled once per day. The atmosphere model is run with fixed sea surface temperature and sea-ice conditions through the day and the various fluxes are accumulated after each atmospheric time step. At the end of the day these fluxes are passed to the ocean model which is then integrated forwards in time and supplies sea surface conditions back to the atmosphere.

2.2 Entropy diagnostics and entropy budget

2.2.1 Entropy diagnostics

The entropy diagnostic used in this study is described in detail in Pascale et al. (2009). The entropy sources of each atmospheric or ocean grid-box are estimated directly from the diabatic heating rates Q_k according to

$$\dot{s}_k = \frac{Q_k}{T} \simeq c_p \frac{1}{T}\frac{\Delta T_k}{\Delta t}\left(\frac{-\Delta p}{g}\right); \qquad [\mathrm{W\ m^{-2}\ K^{-1}}] \qquad (1)$$

where Δt is the physical timestep, c_p the specific heat capacity at constant pressure, Δp the pressure difference between the upper and lower vertical boundaries of the grid-box, ΔT_k the temperature increment after the diabatic process k.

In terms of material sources (1) the global integral rate of material entropy production reads

$$\dot{S}_{mat} = \sum_k \sum_z \int dA c_p \frac{-\Delta p_z}{g}\left(\frac{1}{T}\frac{\Delta T_k}{\Delta t}\right); \qquad [\mathrm{W\ K^{-1}}] \qquad (2)$$

where T is the local temperature at which the heat $c_p(-\Delta p/g)(\Delta T_k/\Delta t)$ is released. The integral is extended over the Earth's surface A and the sums are extended over the vertical model levels z and over all the atmospheric/ocean non-radiative diabatic processes (radiative processes are treated as an external energy source or sink (Goody, 2000; Volk and Pauluis 2010).

We will focus on the material entropy production of the climate system, $\dot{S}_{mat}$, the entropy production associated with dissipation of kinetic energy, $\dot{S}_{diss}$, the planetary entropy production $\dot{S}_{pl}$ (the net entropy flux into space at the top of the atmosphere) and the total dissipated kinetic energy D. Planetary entropy production $\dot{S}_{pl}$ is the net outgoing entropy flux at the top of the atmosphere and it is equal to the total internal entropy production (material + radiation) within the climate system domain. It is approximately estimated by decomposing the outgoing longwave radiation into a sum of contributions $\Lambda_z(x, y)$ of emissions to space from the individual levels z, and dividing each by its temperature $T_z(x, y)$, where x, y is horizontal position. That is:

$$\dot{S}_{pl} = \sum_{z=0}^{N} \int dA \left(\frac{\Lambda_z}{T_z} - \frac{I_{TOA}}{T_{sun}}\right) \qquad (3)$$

where $z = 0$ is the surface, $z = 1, \ldots, N$ the atmospheric levels, I_{TOA} the incoming solar radiation and $T_{sun} = 5777$ K the average brightness of the sun (further details in Pascale et al. 2009). D is diagnosed from the model energy correction heat added back in order to preserve energy conservation in the thermodynamical equation. In Gregory (1998) and Pascale et al. (2009) the energy correction is shown to correspond to the kinetic energy dissipated by turbulent stresses, horizontal hyperdiffusion, gravity wave drag or lost by numerical inaccuracy. As explained in Lorenz (1960, 1967) the kinetic energy dissipated by friction has to equal, on average, the net generation of APE, and the conversion $C(P, K)$ of available potential energy P into kinetic energy K. Therefore $G = C(P, K) = D$ and they are all equivalent measures of the strength of the Lorenz energy cycle. The release in the atmosphere of the heat associated with dissipated kinetic energy leads to the entropy production (Peixoto et al. 1991):

$$\dot{S}_{diss} = \int_V \frac{e}{T}\rho dV. \qquad (4)$$

All these quantities are obtained as global time means over a sufficiently long period in which the system can be considered in a steady state (typically tens of years). If we call $\boldsymbol{\alpha} = (\alpha_1, \alpha_2, \ldots, \alpha_N)$ the set of N internal parameters of the model, all the quantities mentioned above are readily seen as functions of $\boldsymbol{\alpha}$: $\dot{S}_{mat}(\boldsymbol{\alpha})$, $\dot{S}_{diss}(\boldsymbol{\alpha})$, $\dot{S}_{pl}(\boldsymbol{\alpha})$, $D(\boldsymbol{\alpha})$. The standard model configuration is obtained for a specific choice of such parameters $\boldsymbol{\alpha} = \boldsymbol{\alpha}^*$, usually determined by constraining the model output to the observed climatology. Our aim is to explore the variation of $\dot{S}_{mat}, \dot{S}_{diss}, \dot{S}_{pl}, D$ as a function of $\boldsymbol{\alpha}$ and check whether a maximum exists.

2.2.2 Entropy budget

In the control run of the standard setup of FAMOUS (STD), the material entropy production $\dot{S}_{mat} \approx 52 mW\ m^{-2}K^{-1}$ accounts for: (i) dissipation of kinetic energy within the atmosphere ($\approx 13 mW\ m^{-2}K^{-1}$), (ii) temperature hyper diffusion and numerical sources ($\approx 1 mW\ m^{-2}K^{-1}$), (iii) boundary layer sensible heating ($\approx 2 mW\ m^{-2}K^{-1}$), (iv) hydrological cycle ($\approx 37 mW\ m^{-2}K^{-1}$) and (v) ocean diffusion due to small-scale eddies ($\approx 1 mW\ m^{-2}K^{-1}$), as shown in Pascale et al. (2009). $\dot{S}_{mat}$ is thus dominated by the entropy production associated with the hydrological cycle (surface cooling-atmosphere heating), ~70% and kinetic energy dissipation ~ 25%. Therefore we will focus primarily on these two terms. The planetary entropy production $\dot{S}_{pl} = \dot{S}_{mat} + \dot{S}_{rad}$ is a much larger quantity ($\approx 900 mW\ m^{-2}K^{-1}$) but it is dominated by $\dot{S}_{rad}$, that is the entropy production due to shortwave absorption and longwave emission-absorption, which is not counted as part of the internal production of entropy.

2.3 Experimental setup and GCM integration

Modelling uncertainties arise from structural choices made when building the GCM and from the parametrization of processes unresolved at the grid scale. Murphy et al. (2004) studied parameter uncertainties in a large ensemble of climate simulations in order to quantify their impact on climate change predictions. In this study we explore entropy production sensitivity by varying some GCM parameters which Murphy et al. (2004) found to have a strong influence on climate feedback, whose values cannot be accurately determined from observations, and which affect very different climatic processes.

For each parameter choice FAMOUS is run for 100 years. It is observed that the transient period lasts approximately 20–30 years, after which the new climatic state is nearly steady, at least as far the atmosphere and the surface are concerned (total material entropy production depends mainly on the atmospheric state and surface climatology). The deep ocean in fact tends to adjust very slowly and several millennia would be required to spin it up completely. However since the contribution of the interior of the ocean to the total material entropy production is very small (see Sect. 2.2) we can neglect this aspect of the diagnostics, but we do not include parameters controlling ocean physical processes in this study.

For our analysis we have considered only the last thirty years of time integration. Thermodynamical quantities so far discussed are time averaged over such a period and then globally averaged. This was the procedure followed also in FAMOUS systematic tuning (Jones et al. 2005). A list of all the parameters considered in this paper and the ranges over which they are varied is in Table 1. We focus particularly on the convective entrainment rate and the cloud droplet-to-rain conversion rate, because they produce the most interesting results.

3 Experiments with the full AOGCM

3.1 Convective entrainment rate

FAMOUS uses a mass flux convection scheme with representation of cloud ensemble characteristics and stability-dependent closure (Gregory and Rowntree 1990). The entrainment rate coefficient, γ, is a crucial parameter of such a scheme. It sets the fractional mass of entrained dry environmental air, $E = \gamma M$, with M cloud mass flux

Table 1 Some HadCM3 parameters and the physical processes they affect or represent: large scale cloud (LSC), convection (CV), radiation (RAD), boundary layer (BL)

Parameter	GCM component	Process affected	Low	Intermediate	High
V_f (m s^{-1})	LSC	Ice fall speed	0.5	1.0	2.0
c_T (s^{-1})	LSC	Cloud droplet to rain conversion rate	$0.5 \cdot 10^{-4}$	10^{-4}	$4 \cdot 10^{-4}$
RH_c	LSC	Threshold of critical humidity for cloud formation	0.6	0.7	0.9
	CV	Convective entrainment rate: scales rate of mixing between enviromental air and convective plume	0.6	3	9
r_p (μm)	RAD	Effective radius of cloud ice spheres	25	30	40
λ	BL	Asymptotic neutral mixing length parameter: required for calculation of turbulent mixing coefficients	0.05	0.15	0.5
G_0	BL	Boundary layer flux profile parameter: functions used to determine stability dependence of turbulent mixing coefficients	5	10	20
C_h	BL	Charnock constant: roughness lengths and surface fluxes over sea	0.012	0.016	0.020

Parameters range are defined by the "low" and "high" values. Bold font denotes settings in the standard versions (STD). In STD $V_f = 1.747 m\ s^{-1}$. Adapted from Murphy et al. (2004)

(de ned as the amount of air transported in the vertical direction by the cloud, see Gregory and Rowntree 1990 for further details). Several studies have been undertaken to determine the entrainment rate associated with convective plumes. Shallow clouds have ∼ 4 while deep clouds ∼ 1 (Gregory and Rowntree 1990). Thus directly controls the depth of convection (see Fig. 1a–b). In FAMOUS the standard setting is* = 3. The decrease of the entrainment rate coef cient makes convection deeper as well as more narrow whereas the increase of tends to make it more shallow. In fact dry environmental air has the effect of making the moist convective plume drier and more stable, thus reducing its instability and the possibility of keeping rising. This is seen in the diabatic heating (Fig. 1a–b) and temperatures anomalies (Fig. 2a–b).

Figure 3a shows the climate material entropy production $\dot{S}_{mat}(\ )$ and the planetary entropy production $\dot{S}_{pl}(\ )$. The material entropy production and the planetary entropy production have no peak but a monotonic decreasing trend in . They are both thus increasing functions of mean surface temperature. This depends on the fact that is dominated (70%) by the hydrological cycle, whose strength tends to increase with global mean temperature.

In Fig. 3b the dissipation of kinetic energy is shown, $D(\ )$, and the entropy production associated with its dissipation, $\dot{S}_{diss}(\ )$. $D(\ )$ has a maximum for $_M \approx 1{:}5$. The same peak is slightly shifted towards the right for $\dot{S}_{diss}$, which peaks at $_M \approx 1{:}8$, by the effect of the $1/T$ factor in Eq. 4.

3.2 Cloud droplet-to-rain conversion rate c_T

A cloud scheme allowing for layer cloud amount and water content is implemented in FAMOUS (Smith 1990). c_T controls the rate of conversion of cloud liquid water to precipitation $(\dot{q}_L)_P$, which is of the form:

$$(\dot{q}_L)_P = -C\left[c_T\left\{1-\exp\left[-\left(\frac{q_L}{c_W C}\right)^2\right]\right\}+B\right]\frac{q_L}{C} \qquad (5)$$

where C is the mean cloud fraction, q_L the layer cloud water content, $c_W = 8\times10^{-4}$kg kg^{-1} and B (s^{-1}) a constant proportional to the mass ux of precipitation entering the layer from above (for more details see Smith 1990). In the FAMOUS standard con guration $c_T{}^* = 0{:}9414\times 10^{-4}$s^{-1}. The parameter c_T directly affects the liquid and ice water content of clouds (Fig. 4) and the total cloud cover (Fig. 5). Low values (see Table 1) of c_T corresponds to increased cloud cover whereas high values to decreased cloud cover.

In Fig. 1c–d we can see how changes in affect the total diabatic heating and in Fig. 5b how total cloud amount is perturbed. By comparing Fig. 1b with Fig. 1c, Fig. 1a with Fig. 1c, Fig. 2a with Fig. 2d, Fig. 2b with Fig. 2c and Fig. 5a with Fig. 5b, we note that the low values of lead to states

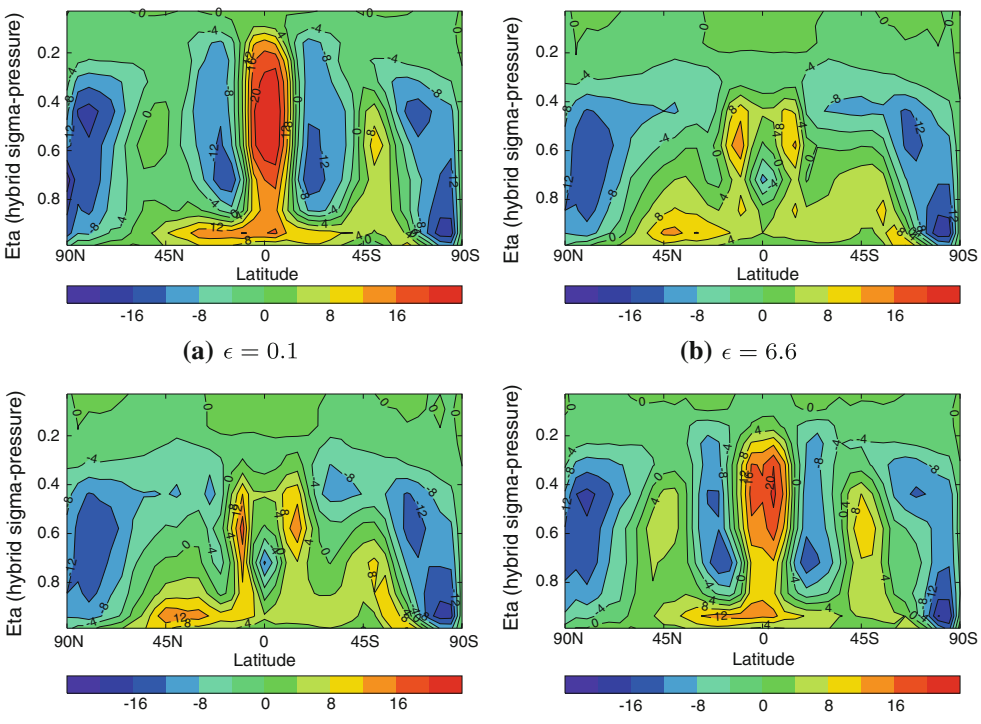

Fig. 1 Total diabatic heating (W m^{-2}) for = 0:1 (a), = 6:6 (b), $c_T = 0{:}3\times10^{-4}$ s^{-1} (c) and $c_T = 6\times10^{-4}$s^{-1} (d). The total diabatic heating includes the contribution from all the physical schemes: cloud scheme, radiation scheme, boundary layer scheme, large scale precipitation scheme and convection scheme

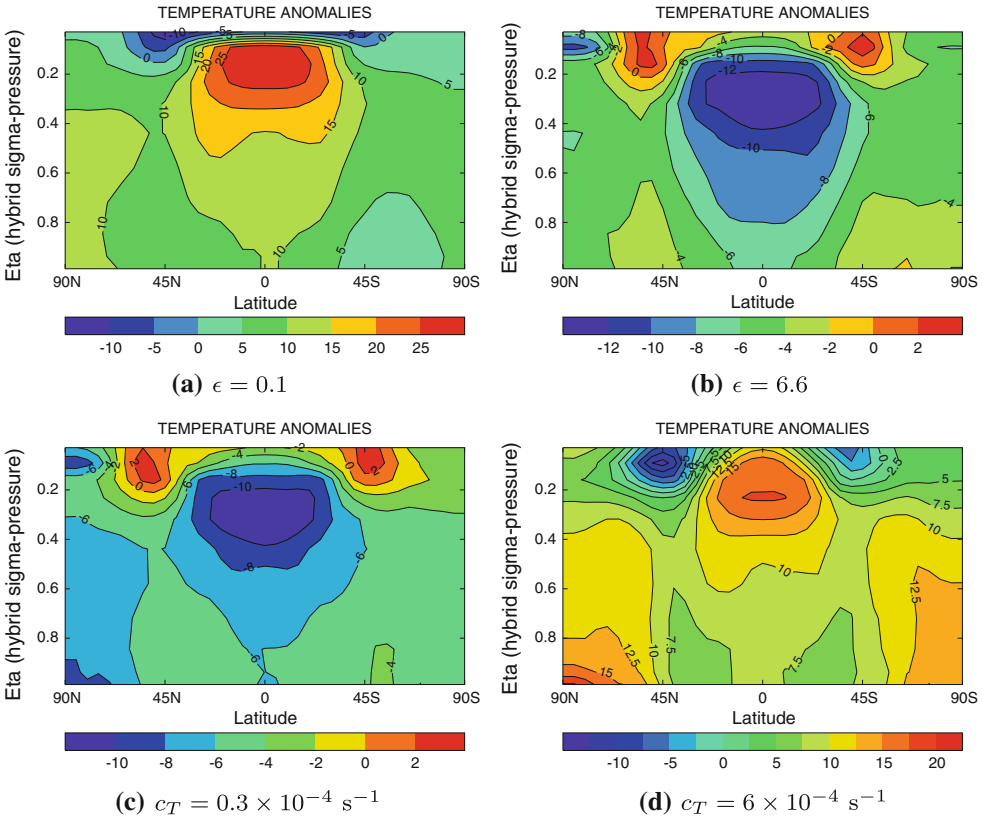

Fig. 2 Temperature anomalies (in K) for $\epsilon = 0.1$ (a), $\epsilon = 6.6$ (b), $c_T = 0.3 \times 10^{-4}$s^{-1} (c) and $c_T = 6 \times 10^{-4}$s^{-1} (d)

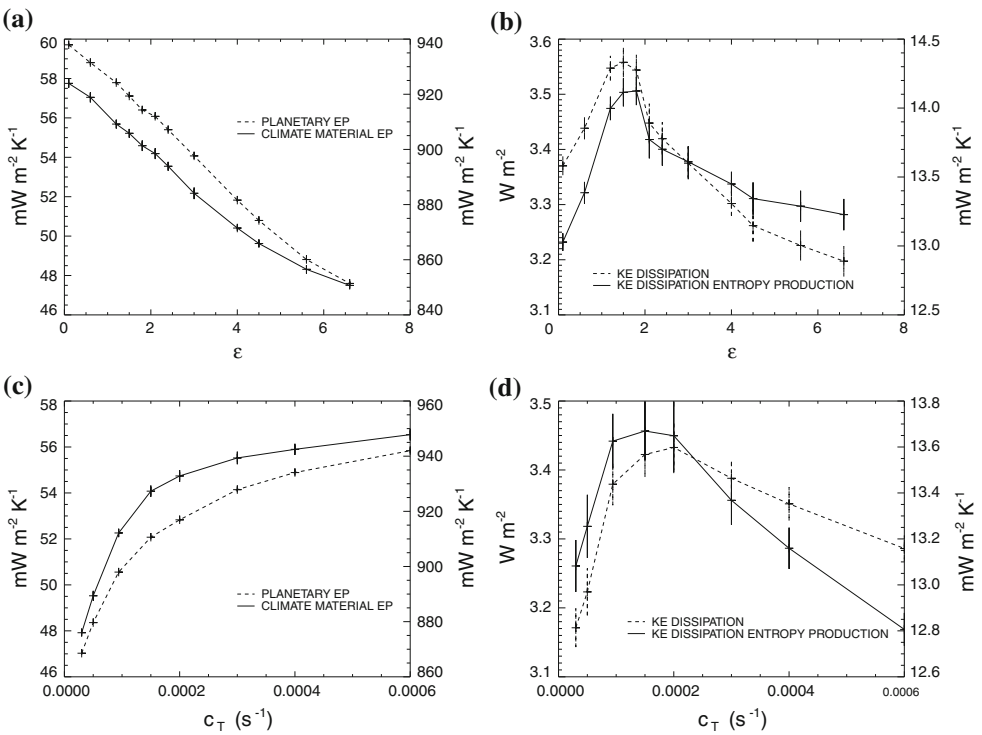

Fig. 3 Planetary entropy production (dashed line, scale on the right axis) and climate material entropy production (continuous line, scale on the left axis) for ϵ variations (a) and c_T variations (c), dissipation of kinetic energy (dashed line, units on the left axis) and entropy production associated with it (continuous line, units on the right axis) for ϵ variations (b) and c_T variations (d). Vertical bars represent interannual variability (±SD, standard deviation of annual means)

resembling the ones obtained for high values of ϵ and vice versa, high values of c_T to states resembling the ones obtained for low values of ϵ. Despite c_T being a fundamentally different parameter from ϵ, their indirect effects on cloud cover and general circulation of the atmosphere are fairly similar, especially at low and mid-latitudes.

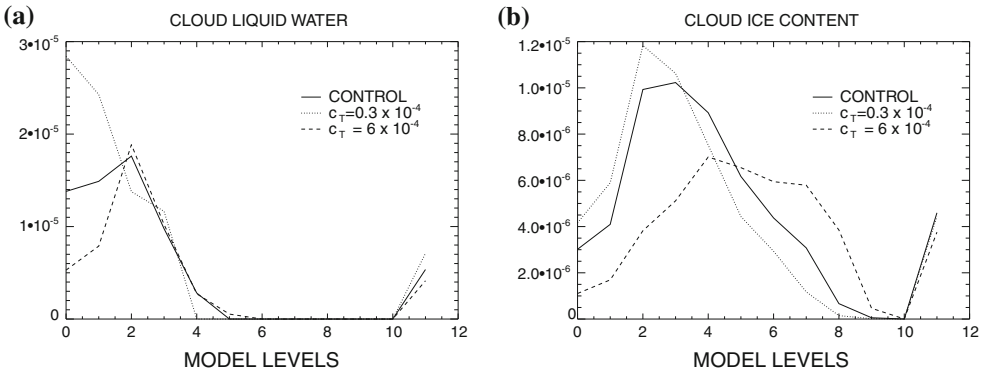

Fig. 4 Variations of cloud liquid water (a) and cloud ice content (b) for $c_T = 0{:}3 \times 10^{-4} s^{-1}$; $c_T = 0{:}9141 \times 10^{-4} s^{-1}$ (control run) and $c_T = 6 \times 10^{-4} s^{-1}$. High values of c_T deplete the water cloud content particularly at the low model levels; conversely low values of c_T are associated with higher cloud water content. High ice cloud is increased by high values of c_T, which promote deeper convection

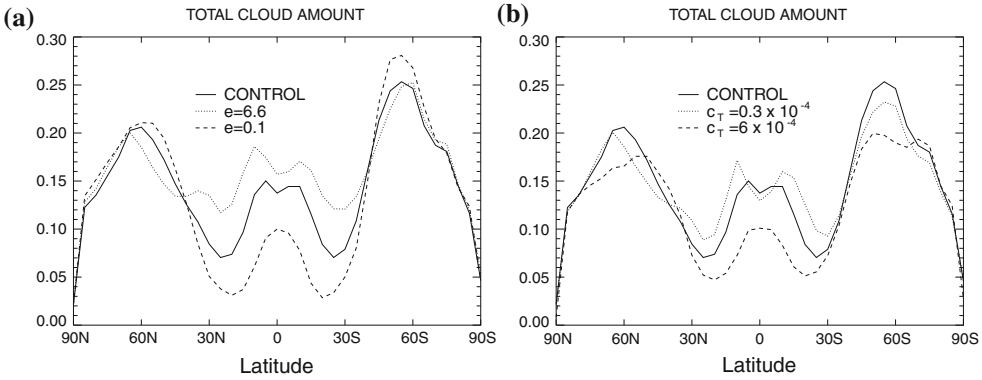

Fig. 5 Vertically averaged cloud amount for c_T variations (b) and variations (a). The two parameters tend to reproduce a similar behaviour in terms of cloud cover

Figure 3d shows $D(c_T)$ and $\dot{S}_{diss}(c_T)$ while in Fig. 3c we present $\dot{S}_{mat}(c_T)$ and $\dot{S}_{pl}(c_T)$. A well-de ned maximum is observed in the dissipation of kinetic energy and in the entropy produced by kinetic energy dissipation, for values of the cloud droplet-to-rain conversion rate between $\times$ 1 $10^{-4} s^{-1}$ and $2 \times 10^{-4}\ s^{-1}$. Again there is no maximum in the total material entropy production of the climate system $\dot{S}_{mat}(c_T)$, which monotonically grows with c_T and temperature and asymptotically approaches a value of about 57mW $m^{-2}K^{-1}$. Likewise the planetary entropy production $\dot{S}_{pl}(c_T)$ levels off around a value of 940 950mW $m^{-2}K^{-1}$.

3.3 Covariation of and c_T

In this second set of simulations the convective entrainment rate, , and the cloud droplet-to-rain conversion rate, c_T, are varied simultaneously. In Fig. 6 the values of $(; c_T)$ chosen are shown by crosses. Covariation of and c_T is examined with the aim of: (i) checking whether the lack of a maximum in $\dot{S}_{mat}$ is a consequence of the one-dimensional reduction onto the axes $=\ ^*$ or $c_T = c_T^*$; (ii) checking whether the maximum in D and $\dot{S}_{diss}$ is significantly shifted in the two dimensional $(; c_T)$-space; (iii) obtaining a wider ensemble of more diverse steady-state climates.

Diagrams in Fig. 6 show D; $\dot{S}_{diss}$; $\dot{S}_{mat}$; $\dot{S}_{pl}$; $T_{1:5}$ and $\mathcal{P}$ as functions of and c_T, where $T_{1.5}$ is the 1.5m atmospheric temperature and $\mathcal{P}$ the total mean precipitation. By examining $T_{1:5}(; c_T)$ we note a "parameter trade-off" direction in the $(; c_T)$ plane, i.e. an increase in and an increase in c_T have balancing effects and the mean surface temperature is fairly constant in this direction. Correspondingly there is a direction "orthogonal" to this last along which the steepest temperature changes occur, and this goes from high , low c_T (shallow convection, more clouds) to low , high c_T (deep convection, less clouds). The contour plots of $\mathcal{P}(; c_T)$ follows very linearly the temperature pattern (linear correlation 0.99) with a percent change of $\mathcal{P}$ vs. $T_{1.5} \sim 2.6\%$ (as usually found in GCM experiments with elevated CO_2 concentration, see for instance Allen and Ingram 2002).

There is no maximum in $\dot{S}_{mat}$ and $\dot{S}_{pl}$, which have a strong linear correlation with $T_{1.5}$ (~ 0.96 for $T_{1.5}$ and ~ 0.90 for $\dot{S}_{pl}$) with a sensitivity of $d\dot{S}_{mat}/dT_{1:5} \sim 0{:}00066$W $m^{-2}K^{-2}$ (1:3%=K, but $\dot{S}_{mat} - \dot{S}_{diss}$ has a percent increase of 1:85%=K), and $d\dot{S}_{pl}/dT_{1:5} \sim 0{:}0046$W $m^{-2}K^{-2}$. For the total material entropy production this is understood in terms of the relation between temperature and the hydrological cycle. As already pointed out (Sect. 2.2), $\dot{S}_{mat}$ is dominated by the surface-atmosphere exchanges of latent and sensible heat uxes which have a :85%=K percent increase. The

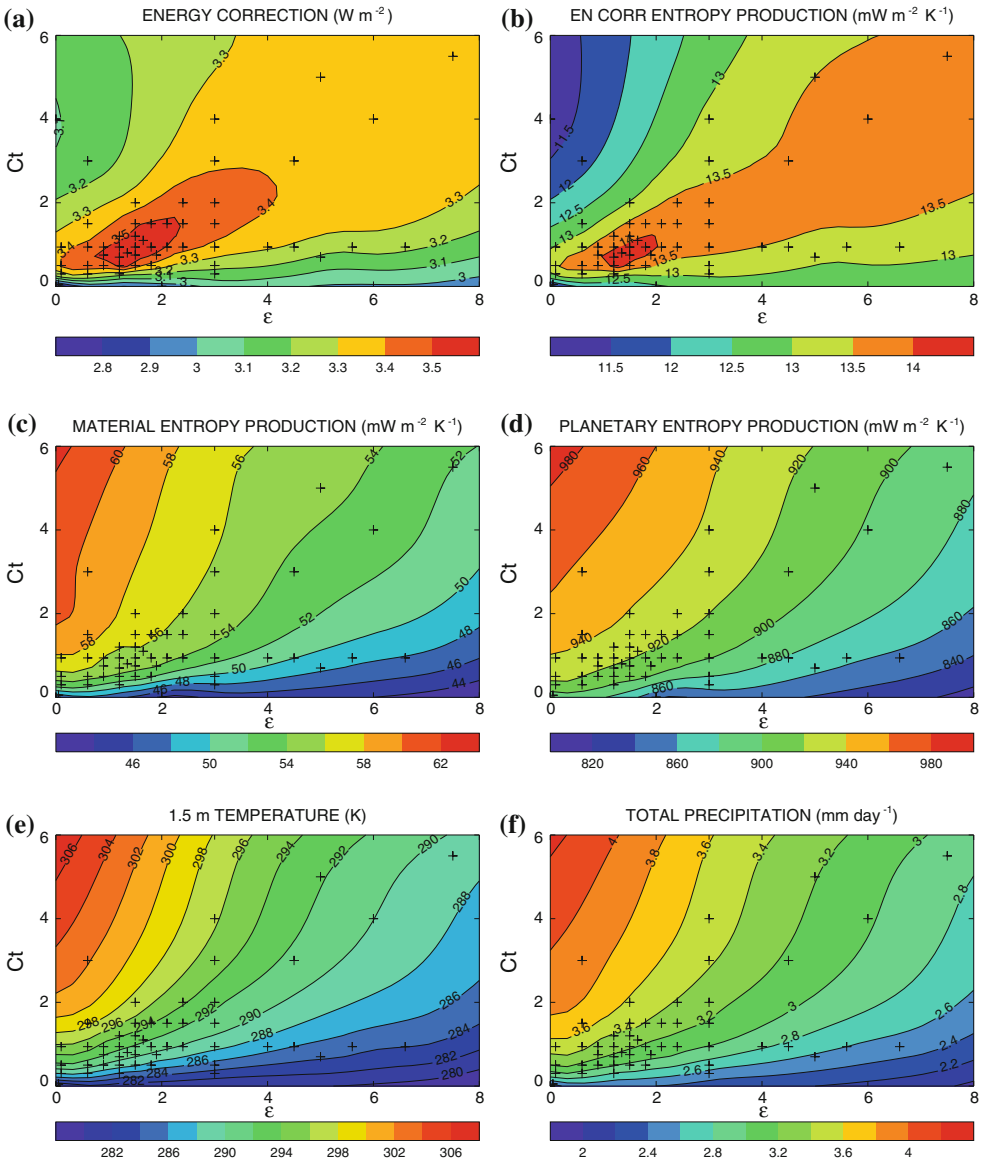

Fig. 6 Diagrams showing a dissipation of kinetic energy (energy correction) (W m^{-2}); b dissipation entropy (mW m^{-2}K^{-1}); c climatic material entropy production (mW m^{-2}K^{-1}); d planetary entropy production (mW m^{-2}K^{-1}); e 1.5m surface temperature (K); f total precipitaion (mm days^{-1}). Crosses indicate the $(\varepsilon; c_T)$ values for which the model has been run. Values have been linearly interpolated using IDL facilities. c_T is in $c_T \times 10^4$ units

increase of planetary entropy production with $T_{1.5}$ is a consequence of the fact that $\dot{S}_{pl} \sim \sigma T_{br}^4 / T_{br}$ (T_{br} Earth's radiative temperature) and $d\dot{S}_{pl}/dT_{1.5} = 3\sigma T_{br}^2 \times dT_{br}/dT_{1.5}$, with $dT_{br}/dT_{1.5} \sim 0.4$.

A completely different pattern characterises $D(\varepsilon; c_T)$ and $\dot{S}_{diss}(\varepsilon; c_T)$. A maximum in D can be seen around $1 \leq \varepsilon \leq 2$ and $0.7 \times 10^{-4} s^{-1} \leq c_T \leq 1.1 \times 10^{-4} s^{-1}$ and likewise for $\dot{S}_{diss}$. Furthermore we observe that there is a whole "band" of values in the $(\varepsilon; c_T)$ plane, from the peak to the top-right corner, with values higher than the surrounding regions. Particularly D and $\dot{S}_{diss}$ drop quite significantly in the direction "orthogonal" to this long ridge, which leads to the most extreme model configurations (low ε-high c_T and high ε-low c_T). Low values of D and $\dot{S}_{diss}$ are found also for low ε and low c_T. The covariation effect does not qualitatively change the results found for the single-parameter experiments but it slightly changes the values at which the peak is reached. In particular the maximum is now obtained for $c_T \sim c_T^*$.

As an independent check we diagnose from model runs the kinetic energy dissipated by the boundary layer stresses, $e_{bl} = 1/\rho(\tau_x \partial_z u + \tau_y \partial_z v)$, where τ_x, τ_y are the turbulent stresses estimated by the boundary layer scheme (Smith 1993) and u, v the zonal and meridional component of the wind. Figure 7 shows the globally averaged values of $\int e_{bl} \rho dV$, in the $(\varepsilon; c_T)$-plane for some of the experiment runs. The boundary layer turbulent stresses directly affect the kinetic field extracting kinetic energy from the large scale flow. In FAMOUS this is modelled as $\partial v/\partial t = \partial \tau/\partial z$ (Smith 1993). It has been shown that e_{bl} accounts for the major part of D (Pascale et al. 2009). Figure 7 shows that a peak in e_{bl} is still found in the same region as for D

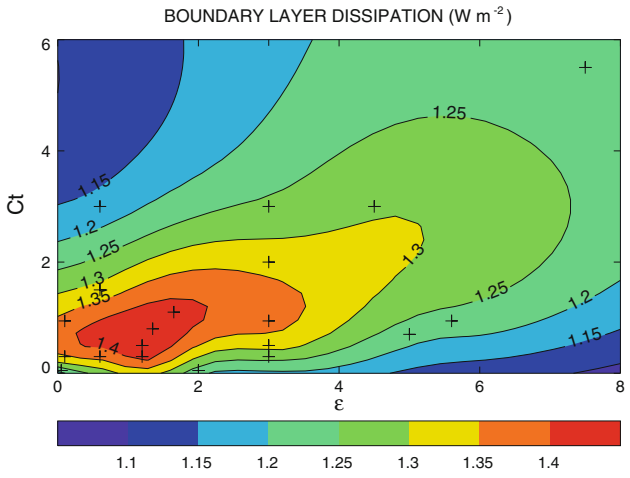

Fig. 7 Kinetic energy dissipated by the boundary layer turbulent stresses as a function of ε and c_T

and $\dot{S}_{diss}$ and the same kind of shape is preserved ("balancing" direction and "steepest" direction). This is in agreement with results by Kleidon et al. (2003, 2006).

A similar non-monotonic behaviour of mean dry static energy, eddy kinetic energy and near-surface eddy kinetic energy (as a measure of surface storminess) in midlatitude baroclinic zones has been recently found by O'Gorman and Schneider (2008) and Schneider et al. (2010) in a series of simulations with an idealised moist general circulation model resulting from changes in longwave optical thickness. In particular the eddy kinetic energy has a maximum for a climate with mean temperature similar to that of present-day earth. Since the eddy kinetic energy, i.e. the kinetic energy not associated with the mean flow but with the midlatitude macroturbulences, tends mostly to be dissipated on a timescale of few days, the result found by O'Gorman and Schneider (2008) is likely to be equivalent to a present-day climate with maximum kinetic energy dissipation.

3.4 Baroclinic activity and the strength of the Lorenz energy cycle

In order to clarify the reasons for the maximum in $D(\varepsilon, c_T)$ let us consider a subset of climates along a path η (Fig. 8) in the (ε, c_T)-space linking two significant and very diverse regions of the (ε, c_T)-space: a "hot climate" ($T_{1.5} \sim 308$ K) in the upper-left part of the diagram and a "cold climate" ($T_{1.5} \sim 275$K) in the lower-right part of the diagram. The path η is through a "maximising" climate ($T_{1.5} \sim 292$K). The climates considered are: (0,4) (hot climate),(0.6,3),(2,1.5), (1.65,1.1) (maximising climate),(1.9,0.75),(3,0.3),(4,0) (cold climate).

The trend in $D(\eta)$ and $e_{bl}(\eta)$ is shown in Fig. 8. $D(\eta)$ and $e_{bl}(\eta)$ scale in the same way, with approximately a 20% drop in hot and cold climate relative to the maximising one. This is consistent with the fact that boundary layer dissipation accounts for about 50 % of the total dissipation in FAMOUS (Sect. 3.3). As discussed in James (1994), the Lorenz energy cycle strength ($G = C(P, K) = D$) is determined by the eddy activity in the midlatitudes since APE is generated mainly zonally in low latitudes but then converted in mid-latitudes into its "eddy" component and hence into eddy kinetic energy, which is dissipated (Lorenz 1955; Boer and Lambert 2008). Classic diagnostics for baroclinic activity are poleward transient eddy temperature fluxes $\overline{v'T'}$ and upward transient eddy temperature fluxes $\overline{-\omega'T'}$ at $600 - 700$ hPa (Hoskins and Valdes 1990). In Fig. 8 we can see that $\overline{v'T'}$ and $\overline{-\omega'T'}$ indexes (area averaged mean over the midlatitude band from 30° to 70°N (S)) and dry static energy $c_p\,T + gz$ have a peak in the maximising climate, dropping for the cold and hot climate. This seems

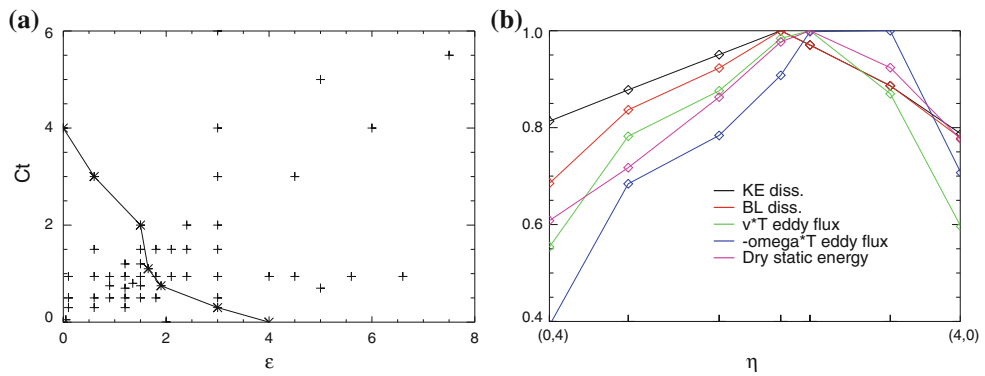

Fig. 8 a Path η in (ε, c_T)-space b Time- and volume-mean of kinetic energy dissipation D, boundary layer kinetic energy dissipation e_{bl}; $\overline{v'T'}$ index, $\overline{-\omega'T'}$ index, dry static energy zonal mean at 50°$\overline{v'T'}$ and $\overline{-\omega'T'}$ indexes are defines as the area averaged mean over the $30° - 70°$N (S) latitudinal region. Quantites are scaled respect to their maximum value (3.55W m^{-2}; 1.42W m^{-2}; 11.3m s^{-1}K; 0.127Pa s^{-1}K and 2PW respectively)

to be in agreement with Kleidon et al. (2003, 2006) and Kleidon (2005), in which it is claimed that the maximum entropy production state is the one with the largest eddy activity in the midlatitudes. This is confirmed by this study providing the primary dissipative function to consider is $\dot{S}_{diss}$ (i.e. G) and not $\dot{S}_{mat}$. Let us note that in moist coupled GCM a state with maximum eddy activity does not necessarily correspond with a state of maximum meridional heat transport as in a dry atmospheric model (Kleidon et al. 2003), since about half of it is due to latent heat which increases with temperature (Schneider et al. 2010) and since cloud feedback may change the net insolation.

3.5 Physical mechanism for the maximum G in

As pointed out by O'Gorman and Schneider (2008) and Hernández-Deckers and Von Storch (2009), changes in eddy kinetic energy or in the Lorenz energy cycle must be related to changes in the atmospheric thermal structure. This in fact affects the mean available potential energy and G, which, as seen in Eq. (6), is proportional to Q (i.e. $\partial T/\partial t$) and T. It is worth therefore trying to understand what are the crucial differences in terms of temperature and diabatic heating in the cold and hot climate respect to the maximising one (see Fig. 9a–b) which lead to a maximum in G, and relate them to physical atmospheric mechanisms. To this aim we estimate G from Lorenz' exact equation:

$$G = \int QN\rho dV \tag{6}$$

where Q is the diabatic heating and $N = 1 - (p_r/p)^k = 1 - T_r/T$ ($k = R/c_p$) is the efficiency factor (Lorenz 1967). The pressure field of the reference state p_r is worked out as the average of p on isentropic surfaces. N is interpreted as the effectiveness of heating at any point in producing APE (Fig. 9c) and where N is negative, cooling will produce APE. This is clear in Fig. 9d, where local contributions to G are shown. It should be kept in mind however that the generation of APE is a global concept. Nevertheless it makes sense to investigate the contributions from different parts of the atmosphere to the global integral because only with such an investigation differences can be explained.

In terms of N and Q, the decrease in G in the case of the hot climate is associated with the redistribution of the diabatic heating (see Fig. 10a–d), particularly in the sub-tropical regions. The tropical convective heating region in fact becomes more narrow and deeper (the tropopause height significantly increases), whereas the sub-tropical subsidence cooling regions shift towards the Equator, leading to negative terms in Eq. (6) (i.e. destruction of APE. Likewise, in hot climate there is an enhanced mid-latitude heating increase at about 50 and 500 hPa height, which corresponds to negative N regions. This creates a negative anomaly in NQ between 20 and 60 which is responsible for a lower APE generation. In contrast, for the cold climate the decrease is essentially a consequence of

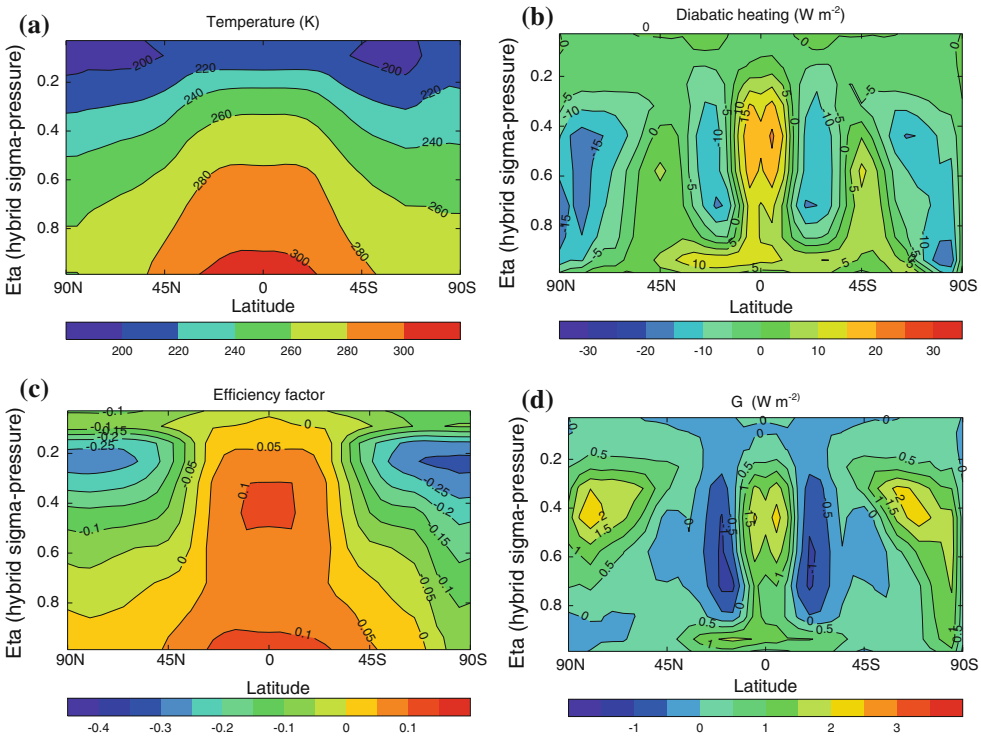

Fig. 9 a Temperature field, b total diabatic heating (mass weighted), c efficiency factor N, d NQ for the maximising climate ($\gamma = 1.65$; $c_T = 1.1 \times 10^{-4} s^{-1}$)

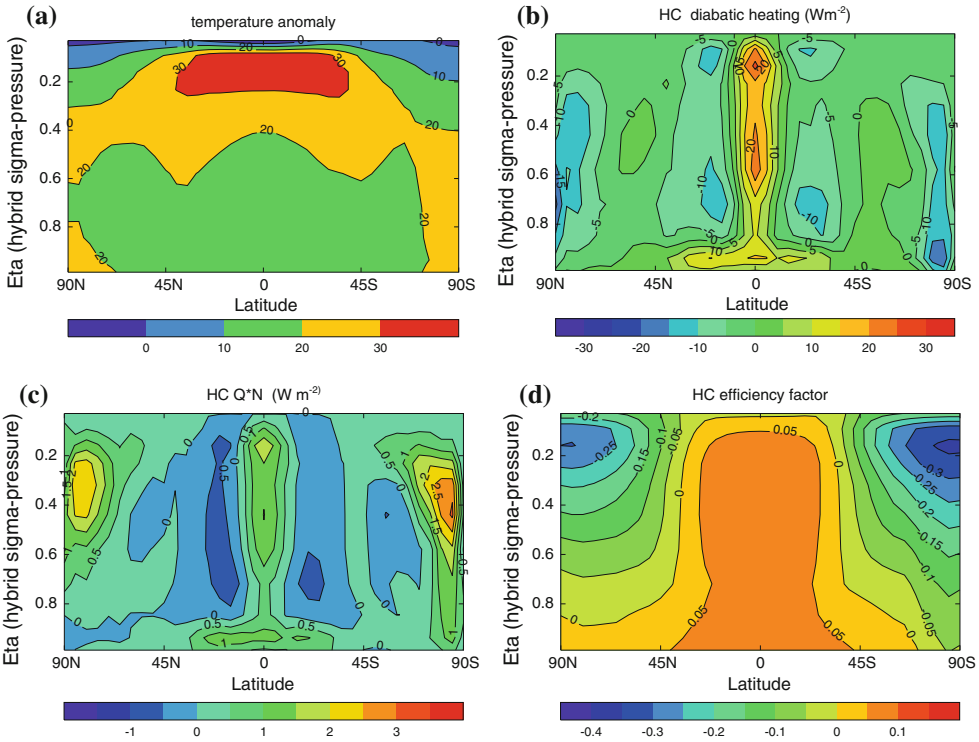

Fig. 10 Hot climate temperature anomalies respect to the maximising climate (a), mass weighted diabatic heating (b), mass weighted N Q (c) and N anomalies (d) respect to the path maximising state

the strong cooling in the tropical upper atmosphere (Fig. 11a–d) associated with the sinking of the tropical tropopause. As a consequence tropical APE generation is greatly reduced.

Another way of understanding the maximum in the Lorenz energy cycle in terms of the thermal structure of the atmosphere is related to the vertical stability and horizontal covariance of T and Q, as suggested by the "approximate" Lorenz' equation (Lorenz 1955):

$$G = \int \gamma \widetilde{T'Q'} \frac{dp}{g} \tag{7}$$

in which $\gamma = -(\theta/T)(R/c_p)(\partial\tilde{\theta}/\partial p)^{-1}$ is an inverse measure of the mean static stability and $\widetilde{T'Q'}$ is the covariance of temperature and diabatic heating over pressure levels (in Eq. 7 $\widetilde{(\cdot)}$ is the mean over a constant pressure surface). Eq. (7) is a very good approximation as shown by Siegmund (1994), with errors smaller than 3% from the exact one (6), and therefore adequately accurate for our purposes. According to Eq. (7), G is given by the covariance of temperature and diabatic heating on pressure levels (horizontal structure of the atmosphere), weighed by the stability factor γ (vertical structure of the atmosphere).

The importance of γ for the energy cycle has already been discussed by Hernández-Deckers and Von Storch (2009), who consider the weakening of the Lorenz energy cycle associated with CO_2-doubling warming. This is due to an overall weakening in the mid-lower atmosphere (associated with an increase in atmospheric stability, i.e. a decrease in γ), having a larger effect than the strengthening in the upper atmosphere (due to the positive heating anomaly). Figure 12b shows the globally-averaged vertical G profile (on model levels), which highlights the decrease below 200 hPa and the increase above in the hot climate.

On the other hand, in the cold climate the weakening of the energy cycle is related to: (a) a general decrease in the temperature covariance in the middle and upper atmosphere ($\leq$450 hPa, Fig. 12d) which dominates the overall increase in γ. This causes G to have no contributions at all from the top model layers ($\leq$350 hPa) and decreased contributions (respect to the maximising climate) between 350 and 450 hPa. In other words we observe a sinking of the stratosphere, with the tropopause now at about 200 hPa, thus leading to lack of heating ($Q \sim 0$), which makes this region of the atmosphere more horizontally uniform and energetically inert; (b) a joint increase in γ and $\widetilde{T'Q'}$ between 750 and 500 hPa which leads to a peak in NQ that, however, does not manage to compensate the strong decrease in the mid-upper atmosphere.

Since we observe that the cold climate has an overall global decrease in $\widetilde{T'Q'}$ and increase in γ, and *vice versa* for the hot climate, with the maximising climate somewhat in the middle, we deduce that the maximum in G must be a

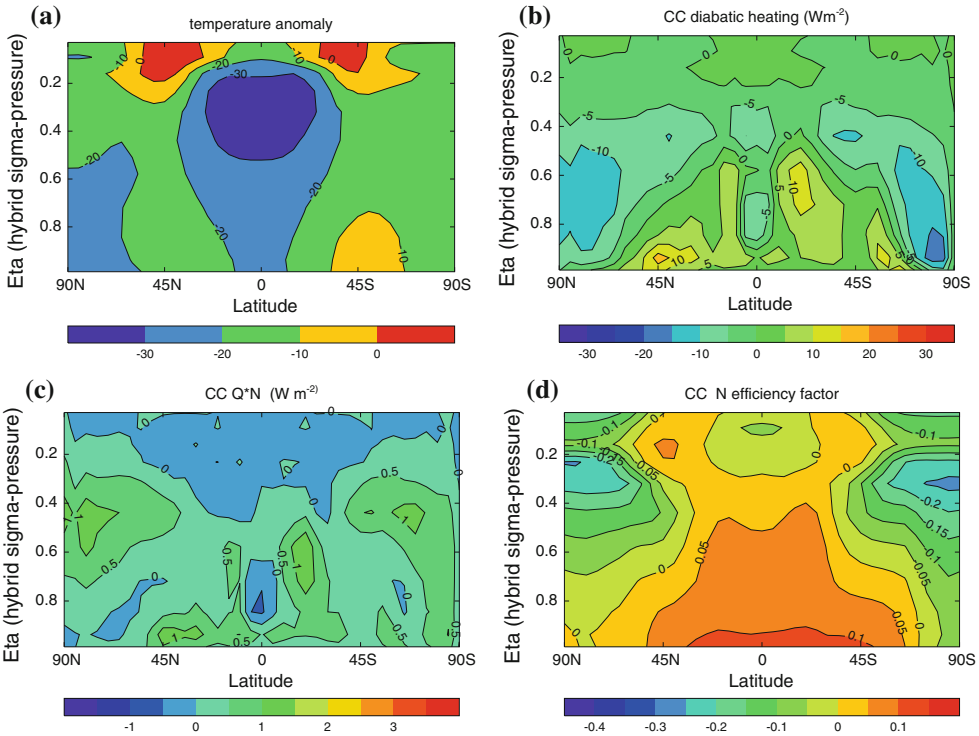

Fig. 11 Cold climate temperature anomalies respect to the maximising climate (a), mass weighted diabatic heating (b), mass weighted NQ (c) and N anomalies (d) respect to the path maximising state

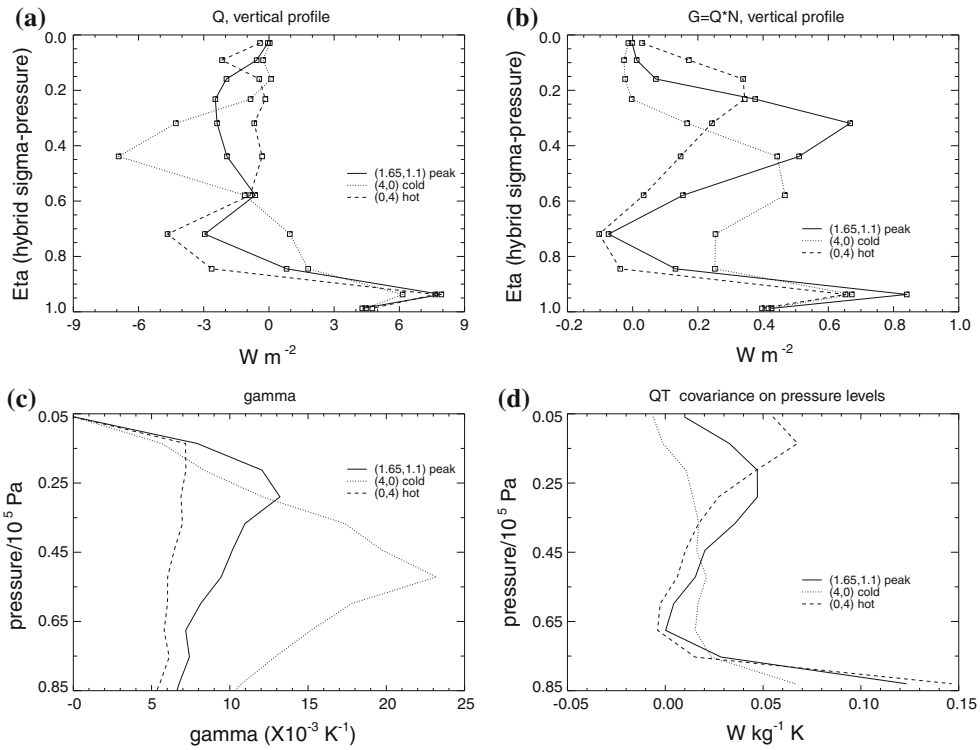

Fig. 12 a Diabatic heating Q; b Generation of APE for model layers for the hot (dashed), maximising (continuous) and cold (dotted) climate; c mean value of γ on pressure levels; d estimated $\widetilde{Q'T'}$ on pressure levels. Eta coordinates are approximately the same as pressure/10^5 Pa

consequence of a trade-off mechanism between γ and $\widetilde{T'Q'}$ in the middle- and upper-atmosphere. There is also a near-surface peak in G (Fig. 12a), due to the diabatic heating of the boundary layer; this is relatively insensitive to climate and does not participate in the trade-off.

3.6 Other parameters

The other parameters listed in Table 1 and considered in Murphy et al. (2004) have also been varied in order to study the entropy sensitivity of the model. For none of them

a "well-behaved" trend (i.e. with a well de ned peak) has been found in G; $\dot{S}_{diss}$; $\dot{S}_{mat}$ or $\dot{S}_{pl}$. Speci cally, RH_c has been varied between 0.5 and 1 and a monotonic increasing behaviour found both in G and $\dot{S}_{mat}$. V_f has been varied between 0.5m s^{-1} and 4m s^{-1} and we nd that G (as well as $\dot{S}_{mat}$) increases quite steeply until a plateau is reached for $V_f \sim 1.5$m s^{-1}, beyond which no substantial change is present. As far as G_0 is concerned (boundary layer ux pro le parameter), a weak monotonic decreasing behaviour is found when varied between 5 and 20 in all the considered thermodynamic quantities. For the remaining parameters λ; C_h; r_p changes in entropy production and rate of production of APE do not show any signi cant trend and their anomalies are within the range of interannual variability.

4 Experiments with xed absorbed shortwave radiation

Although of greater generality, the experiments described so far are hard to compare directly with Kleidon et al. (2003); Kleidon et al. (2006) and the two-box model because in these earlier studies the amount of absorbed shortwave radiation is prescribed, and this is a key element for explaining the results. In order to allow a better comparison we repeat the experiments discussed in Sect. 3 into a simpli ed model setup with xed surface albedo and clouds transparent to longwave and shortwave radiation. This has been achieved: (i) by xing the surface albedo (the sea-ice albedo at its open-sea value and the land albedo at its snow-free value); (ii) by making the clouds transparent to radiation (we set to zero the input stratiform and convective cloud water variables to the radiation code); (iii) by reducing the solar constant from the standard value used in HadCM3, 1,365 W m^{-2}, to 1,215 W m^{-2} (which is equivalent to a superimposed constant increment to planetary albedo) in order to obtain a new steady state with mean surface temperature (288 K) comparable with the standard con guration (289 K). As a consequence the planetary albedo (and hence the net insolation) is prescribed and cannot change with the climatic state obtained for a new choice of the parameter.

The main effect of a constant planetary albedo and no cloud radiative forcing is the reduction of internal variability. For example a reduction of 35% of the standard deviation of annual means is observed in the mean surface temperature and of 27% in the outgoing longwave radiation. All this suggests that global-mean internal variability is strongly in uenced by albedo variability.

A consequence of the fact that in the simpli ed setup clouds are transparent is that the model is now completely insensitive to the parameter r_f, whose direct effect is on the concentration of liquid- and ice- water cloud. Therefore r_f is of no interest in this second idealised experiment. No signi cant sensitivity has been found to V_f; RH_c; λ or G_0; the only remaining parameter of interest is γ.

The model is run for a wider range of γ than before viz. 0.01–20. High values are clearly unphysical (Murphy et al. 2004) but here we just want to use the parametric variation as a way to obtain the most different steady states. The model is still remarkably sensitive to variations of the convective entrainment rate since the distribution of water vapour within the atmosphere affects the radiation scheme (in other words, we have removed the sea-ice and cloud feedback but not the water vapour feedback).

In Fig. 13 the global mean brightness temperature $T_b(\gamma)$ is plotted (which is a measure of the outgoing longwave radiation) and this is fairly constant as expected (if the total solar input is prescribed then, in a steady state, this has to be equal the total amount of outgoing longwave radiation). Despite having a fairly constant mean temperature the climates obtained have different temperature distributions. In Fig. 13 we show the brightness temperature difference between the tropical and extratropical regions. We have de ned as "tropical" the region between 30° S and 30° N and as "extratropical" the union of the regions from 90° S to 30° S and from 30° N to 90° N. Variations in γ produce a variation in the tropics-to-extratropics gradient (in terms of T_b) of about 3 K, with a larger gradient at very low γ.

Figure 13a shows the climate material entropy production and the kinetic energy dissipation. These two quantities have two peaks for $\gamma \sim 15$ and $\gamma \sim 10$ respectively. Are these maxima due to the kind of "trade-off" mechanism as explained in Kleidon (2009) for the 2-box-model? Probably not, but rather to the fact that the variation induced by γ in the climatic uxes and gradients is not monotonic and one-to-one. In other words there may exist a value of γ, say γ_1, above which the poleward heat transport and temperature gradients reverse their direction of change. This can be seen in Fig. 13a, where we have plotted the equator-pole temperature gradient and rate of generation of APE against the poleward atmospheric heat transport. The meridional temperature gradient decreases with the increase of the poleward heat transport and the rate of generation of APE increases. Within the 2-box-model frame (Kleidon 2009, 2004; Lorenz et al. 2001), this means that we are on the left of the maximum in entropy production associated to the meridional heat transport $F(1/T_p - 1/T_e)$ (see Sect. 1). A further increase in poleward heat transport F, and hence a decrease in meridional temperature gradient, would be required to cross the peak. But we observe that γ does not manage to increase the poleward heat transport beyond a value of $\sim$ 3.4 PW; on the contrary, for $\gamma \geq 15$ the poleward heat transport and G decrease, and the meridional temperature gradient increases. This is like going back on

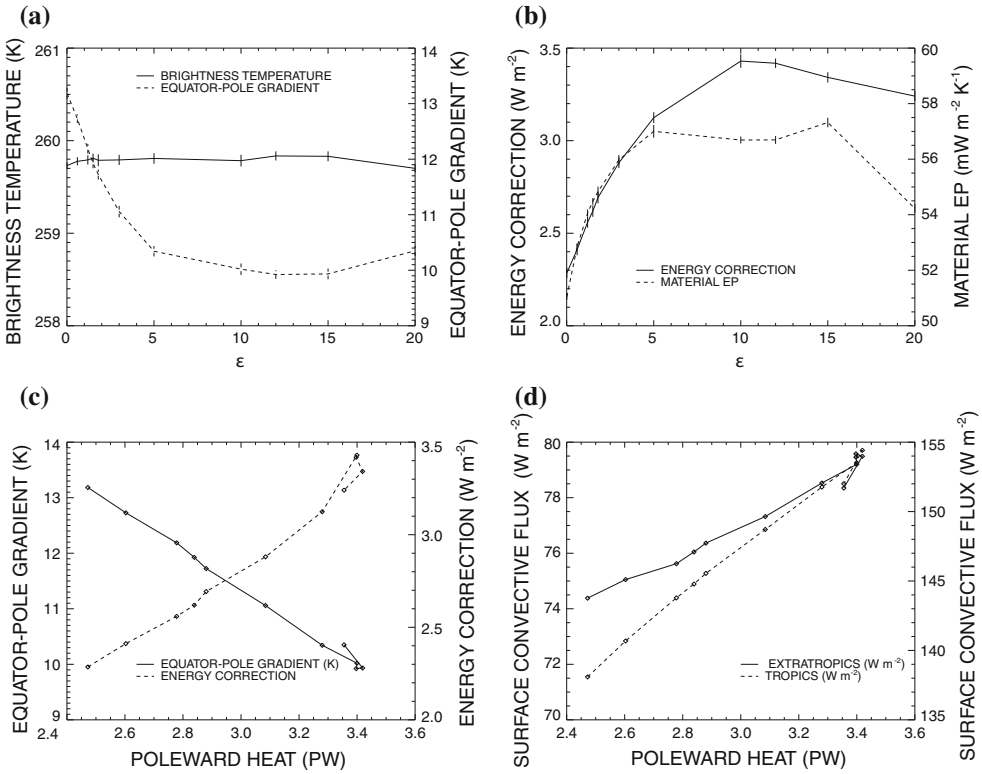

Fig. 13 a Brightness temperature $T_b = (LW/\sigma)^{1/4}$ (LW is the outgoing longwave radiation at the top of the atmosphere) and brightness temperature difference between tropical and extratropical region (dashed line, scale on the right axis); b $\dot{S}_{mat}(\ )$ and $G(\ )$ (continuous line, scale on the left axis); c G (dashed line, scale on the right axis) and equator-pole temperature gradient versus poleward atmospheric heat transport. The poleward heat transport is worked out at 30°S and 30°N and then averaged; d Surface fluxes of latent and sensible heat for tropical (dashed line, scale on the right axis) and extratropical zone

the $F(1/T_p - 1/T_e)$-vs.-F curve (see for example Kleidon 2009, p. 666, Fig. 5) before reaching the maximum. Therefore the maxima we see in Fig. 13b are probably just a consequence of this parametric behaviour and not a "trade-off" maximum in the MEP sense. This kind of "re-folding" is also observed in the surface fluxes of latent and sensible heat (Fig. 13d).

Instead, as in Sect. 3.4, the maximum in G is again associated with the strongest baroclinic activity, as it can be seen by looking at $[\overline{v'T'}]$ and the dry static energy transport at the midlatitudes (not shown). The fact that the MEP and MKED states here correspond to the one with the largest atmospheric poleward heat transport and the smallest equator-pole temperature gradient confirms results by Kleidon et al. (2003) and Kleidon et al. (2006), in which the maximum dissipation state is the most baroclinically active one (and also the one with the maximum entropy production, since in a dry model the entropy production is mostly due to kinetic energy dissipation).

5 Discussion and conclusions

This paper represents the first study of parametric variation aimed at examining MEP in a complex atmospheric-ocean general circulation model, extending previous approaches (Kleidon et al. 2003, 2006; Kleidon 2005; Kunz et al. 2008). Several internal parameters related to sub-grid parametrisations have been considered with particular emphasis on the convective entrainment rate and cloud droplet-to-rain conversion rate.

No maximum in material entropy production is found when parameters are varied. Total material entropy production tends to increase monotonically with absolute temperature thus showing no maxima. The reason for that is the dominance of the entropy production associated with the hydrological cycle (surface evaporation-atmospheric condensation) and the fact that water vapour in air depends strongly on the absolute temperature. This, in turn, is increased by radiative feedbacks associated with changes in clouds induced by parameter variation. From the MEP point of view, the total material entropy production does not seem to be a very interesting quantity in this experiment.

A maximum in the strength of Lorenz energy cycle (measured by either the generation G of available potential energy or the dissipation D of kinetic energy) and in entropy production due to its dissipation is found for values of entrainment rate (~ 2) and cloud droplet-to-rain conversion rate ($c_T \sim 1 - 2 \times 10^{-4} s^{-1}$) inside the range provided by experts (Murphy et al. 2004). This result stands to be a qualitative confirmation of Lorenz's (1960) conjecture and, to a certain extent, of Paltridge's (1978) hypothesis (based on the entropy production associated with the

meridional heat transport only). States of maximum G_m are found to be states of maximum baroclinic activity in agreement with Kleidon et al. (2003); Kleidon et al. (2006). These last results do not hold for any of the remaining parameters considered in Table 1. For some of them (RH_c; V_f; G_0) only monotonic trends are found, for others (λ; C_h) variations in entropy and dissipation are negligible or within the interannual variability. This shows that MEP, even in E. Lorenz' version, cannot be blindly applied to any internal parameter in a GCM.

Experiments are repeated with clear-sky fixed-albedo setup in order to prescribe the net insolation. New climates show a reduced variability and more material entropy production (56 mW m^2 K^{-1} vs. 52 mW m^{-2} K-1 for $T_{1:5} \approx 290$ K) as a consequence of removal of radiative effects of clouds. A maximum in G_m is found corresponding to the maximum meridional heat transfer and minimum temperature gradient, again due to the maximum baroclinic activity. Variation of the meridional heat flux does not manage to show a "trade-off" mechanism for MEP as described in Lorenz et al. (2001) and Kleidon (2009). This demonstrates that in complex, highly constrained models changes to basic climatic fluxes and gradients deriving from parameter perturbations may not detect MEP, as questioned by Goody (2007). Nevertheless results seem to be in agreement with Kleidon's explanation of MEP states as states of maximum atmospheric poleward heat transport (Kleidon et al. 2003, 2006; Kleidon 2005).

This paper explores the limits of applicability of the MEP and MKED when models become complex and highly constrained by many equations (as is the case for GCMs) but still preserve a degree of uncertainty linked to the parametrisations. Such an uncertainty, which arises from our ignorance of sub-grid scales, has consequences for the large scale circulation, producing a wide range of different climate states. MEP provides an effective tuning methodology for earth system models of intermediate complexity (EMICs) and simple atmospheric circulation models while still little is known of its utility for complex GCMs. Results from this work show a qualitative confirmation of MKDE which looks to be a more fruitful concept than MEP. Therefore the two concepts may be inherently different in complex climate systems (and in the real world). This seems to match recent concerns by Paltridge (2001) and Goody (2007) who argue that the focus on the energetics of turbulent medium rather than the concept of entropy production may be more relevant for an extremum principle and closer to the traditional thinking of the atmospheric community (Malkus 2003). Conversely, by considering Dewar's view on MEP as valid (Dewar 2009), the apparent failure of MEP in our results may point out a missing constraint in the application of MEP to atmospheric dynamics.

Acknowledgments Salvatore Pascale thanks Robin Smith for the help provided with FAMOUS experiments and Valerio Lucarini for helpful comments. Jonathan Gregory is supported by the NCAS-Climate Programme and the Joint DECC and Defra Integrated Climate Programme, DECC/Defra (GA01101).

References

Allen MR, Ingram WJ (2002) Constraints on future changes in climate and the hydrological cycle. Nature 419:224–232

Ambaum MHP (2010) Thermal physics of the atmosphere. Wiley, Chichester, 256pp

Bejan A, Lorente S (2004) The constructal law and the thermodynamics of flow systems with configuration. Int J Heat Mass Transf 47:3203–3214

Boer GJ, Lambert S (2008) The energy cycle in the atmospheric model. Clim Dyn 30:371–390

Cullen MJP, Davies T (1991) A conservative split-explicit integration scheme with fourth order horizontal advection. Q J R Meteorol Soc 117:993–1002

Dewar RC (2005) Maximum entropy production and the fluctuation theorem. J Phys A 38:L371–L381

Dewar RC (2009) Maximum entropy production as an inference algorithm that translates physical assumption into macroscopic predictions: don't shoot the messenger. Entropy 11:931–944

Edwards JM, Slingo A (1996) Studies with a flexible new radiation code. part one: choosing a configuration for a large-scale model. Q J R Meteorol Soc 122:689–719

Egger J (1999) Numerical generation of entropies. Mon Weather Rev 127:2211–2216

Fraedrich K, Lunkeit F (2008) Diagnosing the entropy budget of a climate model. Tellus A 60(5):921–931

Fraedrich K, Jansen H, Kirk E, Luksch U, Lunkeit F (2005) The planet simulator: towards a user friendly model. Meteorol Z 14:299–304

Fraedrich K, Kirk E, Luksch U, Lunkeit F (2005) The portable university model of the atmosphere (PUMA): storm track dynamics and low-frequency variability. Meteorol Z 14:735–745

Goody R (2000) Sources and sinks of climate entropy. Q J R Meteorol Soc 126:1953–1970

Goody R (2007) Maximum entropy production in climate theory. J Atmos Sci 64:2735–2739

Gordon C, Cooper C, Senior CA, Banks H, Gregory JM, Johns TC, Mitchell JFB, Wood RA (2000) The simulation of SST, sea ice extents and ocean heat transports in a version of the Hadley Centre coupled model without flux adjustments. Clim Dyn 16:147–168

Grassl H (1981) The climate at the maximum-entropy production by meridional atmospheric and oceanic heat fluxes. Q J R Meteorol Soc 107:153–166

Gregory D (1995) A consistent treatment of the evaporation of rain and snow for use in large-scale models. Mon Weather Rev 123:2716–2732

Gregory D (1998) Unified model documentation paper no. 28. Technical report, Meteorological Office

Gregory D, Rowntree PR (1990) A mass flux convection scheme with representation of cloud ensemble characteristics and stability-dependent closure. Mon Weather Rev 118:1483–1506

Grinstein G, Linsker R (2007) Comments on a derivation and application of the maximum entropy production principle. J Phys A 40:9717–9720

Hernández-Deckers D, Von Storch J (2009) Energetics responses to increases in greenhouse gas concentration. J Clim 23:3874–3887

Hoskins BJ, Valdes PJ (1990) On the existence of storm-tracks. J Atmos Sci 47(15):1854–1864

James IN (1994) Introduction to circulating atmosphere. Cambridge University Press, Cambridge
Johnson DR (1997) "General Coldness of Climate Models" and the second law: implications for modelling the earth system. J Clim 10:2826–2846
Jones C, Gregory J, Thorpe R, Cox P, Murphy J, Sexton D, Valdes P (2005) Systematic optimisation and climate simulation of FAMOUS, a fast version of HadCM3. Clim Dyn 25:189–204
Kleidon A (2004) Beyond gaia: thermodynamic of life and earth system functioning. Clim Change 66:271–319
Kleidon A (2005) Hyperdiffusion, maximum entropy production, and the simulated equator-pole temperature gradient in an atmospheric general circulation model http://hdl.handle.net/1903/1927
Kleidon A (2009) Nonequilibrium thermodynamics and maximum entropy production in the earth system. Naturwissenschaften 96:653–677
Kleidon A (2010) Life, hierarchy and the thermodynamic machinery of planet Earth. Phys Life Rev (in press)
Kleidon A, Fraedrich K, Kunz T, Lunkeit F, (2003) The atmospheric circulation and the states of maximum entropy production. Geophys Res Lett 30(23)
Kleidon A, Fraedrich K, Kirk E, Lunkeit F (2006) Maximum entropy production and the strenght of boundary layer exchange in an atmospheric general circulation model. Geophys Res Lett 33(L06706):4. doi 10.1029/2005GL025373
Kunz T, Fraedrich K, Kirk E (2008) Optimisation of simpli ed GCMs using circulation indices and maximum entropy production. Clim Dyn 30:803–813
Lorenz EN (1955) Available potential energy and the maintenance of the general circulation. Tellus 7:271–281
Lorenz EN (1960) Generation of available potential energy and the intensity of the general circulation. Pergamon, Tarrytown
Lorenz EN (1967) The nature and theory of the general circulation of the atmosphere, volume 218.TP.115. World Meteorological Organization
Lorenz RD, Lunine JI, Withers PG, McKay CP (2001) Titan, mars and earth: entropy production by latitudinal heat transport. Geophys Res Lett 28(3):415–418
Lucarini V (2009) Thermodynamic ef ciency and entropy production in the climate system. Phys Rev E 80:021118. doi 10.1103/PhysRevE.80.02118
Lucarini V, Fraedrich K, Lunkeit F (2010) Thermodynamic analysis of snowball earth hysteresis experiment: ef ciency, entropy production and irreversibility. Q J R Meteorol Soc 136:1–11
Lucarini V, Fraedrich K, Lunkeit F (2010b) Thermodynamics of climate change: generalized sesnitivities. Atmos Chem Phy 10:9729–9737. doi 10.5194/acp-10-9729-2010
Malkus WVR (2003) Borders of disordrs: in turbulent channel ow. J Fluid Mech 489:185–198
Martyushev LM, Seleznev VD (2006) Maximum entropy production principle in physics,chemistry and biology. Phys Rep 426:1–45
Murakami S, Kitoh A (2005) Euler-lagrange equation of the most simple 1-D climate model based on the maximum entropy production hypothesys. Q J R Meteorol Soc 131(608):1529–1538
Murphy JM, Sexton DMH, Barnett DN, Jones GS, Webb MJ, Collins M, Stainforth DA (2004) Quanti cation of modelling uncertainties in a large ensemble of climate change simulations. Nature 430:768–772
Noda A, Tokioka T (1983) Climates at minima of the entropy exchange rate. J Meteorol Soc Jpn 61:894–908
Odum HT (1988) Self-organization, transformity and information. Sci Agric 242:1132–1139
O'Gorman PA, Schneider T (2008) Energy of midlatitude transient eddies in idealized simulations of changed climates. J Clim 21:5797–5808. doi 10.1175/2008JCLI2099.1
Ozawa H, Ohmura A (1997) Thermodynamics of a global-mean state of the atmosphere: a state of maximum entropy increase. J Clim 10:441–445
Ozawa H, Ohmura A, Lorenz R, Pujol T (2003) The second law of thermodynamics and the global climate system: a review of the maximum entropy production principle. Rev Geophys 41(1018):24. doi 10.1029/2002RG000113
Paltridge GW, Farquhar GD, Cuntz M (2007) Maximum entropy production, cloud feedback, and climate change. Geophys Res Lett 34(L14708):6. doi 10.1029/2007GL029925
Paltridge GW (1975) Global dynamics and climate-a system of minimum entropy exchange. Q J R Meteorol Soc 101:475–484
Paltridge GW (1978) The steady state format of global climate. Q J R Meteorol Soc 104:927–945
Paltridge GW (2001) A physical basis for a maximum of thermodynamic dissipation of the climate system. Q J R Meteorol Soc 127:305–313
Pascale S, Gregory JM, Ambaum M, Tailleux R (2009) Climate entropy budget of the HadCM3 atmosphere-ocean general circulation model and FAMOUS, its low-resolution version. Clim Dyn. doi:10.1007/s00382–009–0718–1
Pauluis O, Held IM (2002a) Entropy budget of an atmosphere in radiative-convective equilibrium. Part I: maximum work and frictional dissipation. J Atmos Sci 59:125–139
Pauluis O, Held IM (2002b) Entropy budget of an atmosphere in radiative-convective equilibrium. Part II: latent heat transport and moist processes. J Atmos Sci 59:140–149
Peixoto JP, Oort AH, de Almeida M, Tomé A (1991) Entropy budget of the atmosphere. J Geophys Res 96(D6):10981–10988
Pope VD, Gallani ML, Rowntree PR, Stratton RA (2000) The impact of new physical parametrizations in the Hadley Centre climate model–HadAM3. Clim Dyn 16:123–146
Pujol T, Fort J (2002) States of maximum entropy production in a one-dimensional vertical model with convective adjustments. Tellus A 54:363–369
Reichler T, Kim J (2008) How well do coupled models simulate today's climate?. Bull Am Meteorol Soc 89:303–311
Rodgers CD (1976) Minimum entropy exchange principle-reply. Q J R Meteorol Soc 102:455–457
Schneider T, O'Gorman PA, Levine XJ (2010) Water vapor and the dynamics of the climate changes. Rev Geophys 48(RG3001):22. doi:10.1029/2009RG000302
Schulman LL (1977) A theoretical study of the ef ciency of the general circulation. J Atmos Sci 34:559–580
Siegmund P (1994) The generation of available potential energy, according to Lorenz' exact and approximate equations. Tellus 46(A):566–582
Smith RNB (1990) A scheme for predicting layer clouds and their water content in a general circulation model. Q J R Meteorol Soc 116:435–460
Smith RNB (1993) Uni ed model documentation paper no. 24. Technical report, Meteorological Of ce
Smith RS, Gregory JM, Osprey A (2008) A description of the FAMOUS (version xdbua) climate model and control run. Geosci Model Develop 1:147–185
Tailleux R (2010) Entropy versus APE production: on the buoyancy power input in the oceans energy cycle. Geophys Res Lett 37(L22603). doi 10.1029/2010GL044962
Volk T, Pauluis O (2010) It is not the entropy you produce, rather, how you produce it. Philos Trans R Soc B 365:1317–1322. doi: 10.1098/rstb.2010.0019
Wang B, Nakajima T, Shi G (2008) Cloud and water vapor feedbacks in a vertical energy-balance model with maximum entropy production. J Clim 21(24):6689–6698